LABORATORY EXPOSURE LOOP FOR SIMULATION OF FOSSIL FUEL POWER PLANT SUPERHEATER OPERATION CONDITIONS

[1,2]Lucie PILSOVÁ, [2]Marie OHANKOVÁ, [1]Vladimír MÁRA, [2]Irena ANDRŠOVÁ

[1]UJP PRAHA a.s., Prague, Czech Republic, EU, pilsova@ujp.cz, ohankova@ujp.cz, andrsova@ujp.cz

[2]CTU in Prague, Faculty of Mechanical Engineering, Department of Materials Engineering, Prague, Czech Republic, EU, vladimir.mara@fs.cvut.cz

https://doi.org/10.37904/metal.2024.4935

Abstract

The article deals with the first results from the so-called laboratory exposure loop after 10,000 h operation. This loop is an experimental setup that allows the selected material to be exposed to the conditions that prevail in the boiler of a coal-fired power plant or incineration site. Among these conditions are elevated temperature, corrosive environment, and internal pressure of water steam. In this case, the loop (consisting of two bends and six weld joints) was made from SUPER 304H (X10CrNiCuNb18-9-3) superheater tubes. Before the experiment, the welded loop was filled with water, so steam with a pressure of 23 MPa was generated when heated to 550 °C. In addition, small-scale, stripe-shaped specimens were placed inside the loop and then exposed to steam during exposure. The loop was placed partly out of the furnace, thus not fully heated, and covered up with the power plant ash. At weekly intervals, the cooler part of the loop (the one covered up with the ash) was sprayed with water to induce thermal shock. After exposure of both loops (one for 5000 h, the other for 10,000 h), their bodies were cut, and mechanical tests (i.e. tensile and Charpy impact tests) were performed. The microstructure of the straight parts bends and weld joints of the loop tubes was investigated 1and documented using light optical microscopy (LOM) and scanning electron microscopy (SEM).

Keywords: Exposure loop, austenitic steel, SUPER 304H, superheater, microstructure

1. INTRODUCTION

Currently, coal-fired power plants operating in the Czech Republic are listed as the first to be shut down due to decarbonization. However, it still accounts for about half of the total installed capacity of the Czech Republic. With the gradual decline of coal-fired heat and power generation, the reliability of the operation of the reconstructed facilities will continue to gain importance. As presented by representatives of the Ministry of Industry and Trade of the Czech Republic in mid-May 2024, the currently being prepared legislative strategy includes ensuring the safe operation of the electricity system during a controlled shift away from coal [1,2].

When switching to other than fossil energy sources, it will still be necessary to have facilities in reserve capable of replenishing energy capacities at defined times and balancing the electrical network for this transition period. The materials in these backup sources will already have a certain degradation history behind them which will be followed by irregular starts to full power. In this paper, new approaches to laboratory simulation of material degradation from steam superheater piping systems operating at 550 °C/20 MPa and above are presented and discussed. Since the device is a modular system, practically any material can be used, from which a loop of suitable dimensions can be made and exposed at the selected parameters of temperature and steam pressure.

2. EXPERIMENTAL MATERIAL AND METHODS

2.1. Materials and methods

SUPER 304H steel superheater tubes (outer diameter *OD* = 38 mm and wall thickness *t* = 3.6 mm) in the form of straight tubes and R60 bends in the unannealed state after bending were selected for the experiment. The welding joints were made in two ways, with an automated orbital head using the TIG method with the filler material Thermanit 304HCu, corresponding to the composition of the base material, and manually using the TIG method with Ni-based filler material UTP A 6170 Co. The chemical composition is given in **Table 1**.

Table 1 Nominal chemical composition (wt%) of experimental materials [3]

Material	C	Si	Mn	P	S	Cr	Ni	Cu	Mo	Nb	B	N	Al	Co	Ti	Fe
SUPER 304H	0.07-0.13	<0.30	<1.00	<0.040	<0.010	17.0-19.0	7.5-10.5	2,5-3,5	-	0.30-0.60	0.001-0.010	0.05-0.12	0.003-0.030	-	-	Bal.
Thermanit 304HCu	0.1	0.4	3.2	-	-	18.0	16.0	3.0	-	0.4	-	0.2	-	-	-	Bal.
UTP A 6170 Co	0.06	<0.3	-	-	-	22.0	Bal.	-	8.5	-	-	-	1.0	11.5	0.4	1.0

Standard metallographic procedures were used for the analysis – cutting on a band saw and then on a metallographic cutting machine, fixing in epoxy or conductive carbon resin, grinding on SiC papers, mechanical polishing, and electrolytic etching in a 10 % aqueous solution of oxalic acid. The structure was documented using Nikon Eclipse MA200 and Olympus DSX1000 light microscopes and a JEOL JSM-7600F scanning electron microscope with an Oxford X-Max 80 mm^2 Energy-dispersive X-ray Spectroscopy (EDS) detector. Tensile tests were performed on short proportional cylindrical rods with d_0 = 5 mm and a M8 incomplete thread on an Instron 5582 universal test machine. The HV1 hardness maps were measured using a Struers Duramin 40AC3 automatic hardness tester

2.2. Experimental setup

In this case, the laboratory equipment was assembled from two chambers. The first chamber (laboratory resistance furnace) serves to create as homogeneous temperature field as possible in the air. The second chamber models the corrosion environment in the ash from the power plant. Both chambers are connected by a test body. The basis is a closed ellipsoid in which superheated steam was created. Internal specimens were inserted into this ellipsoid. The shell of the ellipsoid was to be stressed by the internal pressure of superheated steam, temperature and, in one chamber, also by corrosively aggressive ash, in which part of the ellipsoid was placed. The ellipsoid was designed in the form of a weld, as shown in **Figure 1** with four internal specimens (see the partial radiograph in the upper left corner of **Figure 1**).

Figure 1 The exposure loop. On the left bend B (in the furnace) with an example of an X-ray image of the inner body, on the right bend A (corrosion ash).

3. RESULTS AND DISCUSSION

3.1. Tensile test

The exposure loop was operated for 10,000 hours at a nominal temperature of 550 °C and an internal overpressure of 23.2 MPa. The bend marked B was placed in the furnace, the bend A was placed in the corrosive ash. The loop body was cut and for the purposes of this article a tensile test was performed on all welds. Rings were cut from the tops of both bends for documentation using light and electron microscopy.

The tensile test at room temperature of the weld joints marked A, C and E (where A with the lowest exposure temperature and weld E closest to weld B, located in the furnace) did not show significant differences in the values of the offset yield strength and ultimate strength. The average value of the 0.2 % offset yield strength was $R_{p0.2}$ = (470±17) MPa and the ultimate strength R_m = (655±17) MPa. The average plastic properties were represented by elongation A = (19.9±1.5) % and contraction Z = (61.9±6.8) %. The unexposed weld joint in [4] showed: $R_{p0.2}$ = 338 MPa, R_m = 642 MPa, A = 53.3 % and Z = 79.0% - see **Figure 2**.

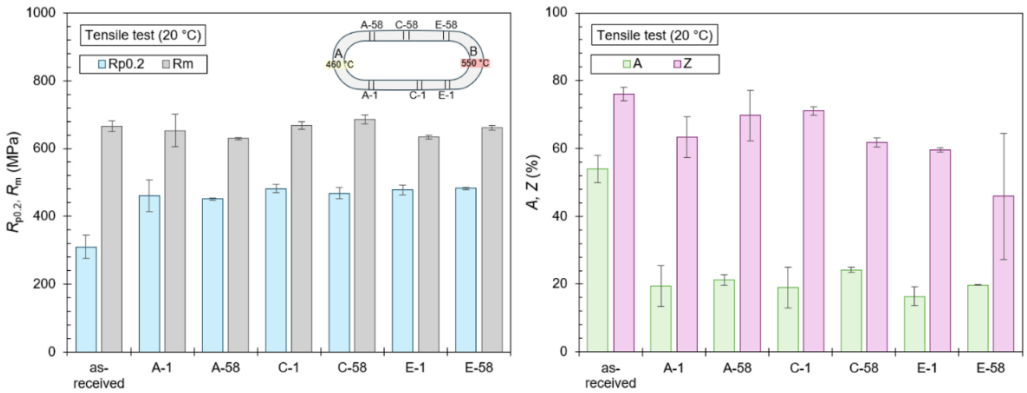

Figure 2 Results of the tensile test of weld joint samples from the exposure loop

3.2. Fractography

Failure of all weld joints occurred in the weld metal with a transition to the heat-affected zone. **Figure 3** shows pictures of fracture surfaces that did not show a purely dendritic failure character. More atypical phenomena were observed in manual weld joints than in joints made with an orbital welding head.

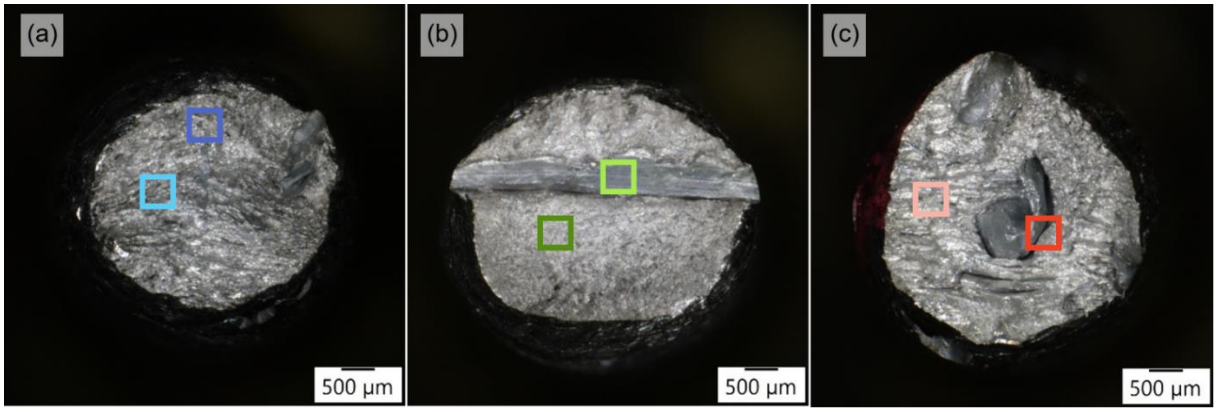

Figure 3 Macroimages of the fracture areas after tensile test of (a) weld A-1, (b) weld C-1 and (c) weld E-1

The areas marked with colored rectangles in **Figure 3** were documented in more detail using SEM, as shown in **Figure 4**. In all cases, transgranular ductile failure with characteristic dimples around small precipitates occurred. In the case of images in **Figure 4**b, d and f, the nature of the fracture was mixed. In the dendritic structure of the weld metal, partial cleavage failure was observed. An EDS point analysis of the chemical

composition performed in the area in **Figure 4**e showed that the centered inclusion is an iron oxide also containing Cr and Ni, and was, concerning its size, probably formed during welding.

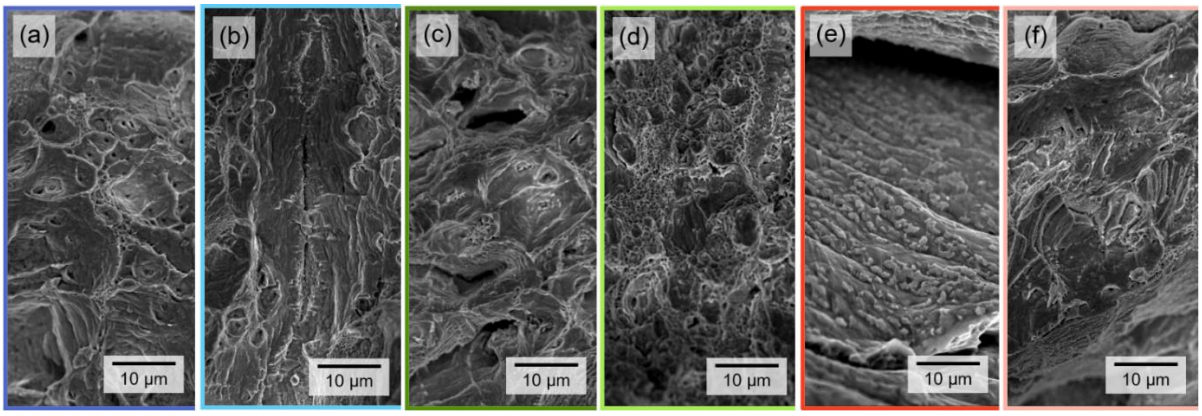

Figure 4 SEM images of the fracture areas marked in Figure 3;
(a), (b) weld A-1; (c), (d) weld C-1 and (e), (f) weld E-1

3.3. Microstructure

The base material of SUPER 304H steel contains polyhedral austenitic grains of size G 9 with primary hardening particles of the type NbC or NbCN evenly distributed in the matrix. As a result of exposure at 550 °C (only 460 °C in the case of the end in corrosion ash), there is a gradual occupation of the grain boundaries by precipitates, which, according to further analyses, have been proven to be $M_{23}C_6$ carbides. As can be seen in **Figure 5**, the grain boundaries in the core of the tension side of the bends were more intensively occupied by carbides in the case of bend B, which was operated at a higher temperature. The most deformed grains were observed near the surface of the outer diameter (**Figure 5**a and **Figure 5**c).

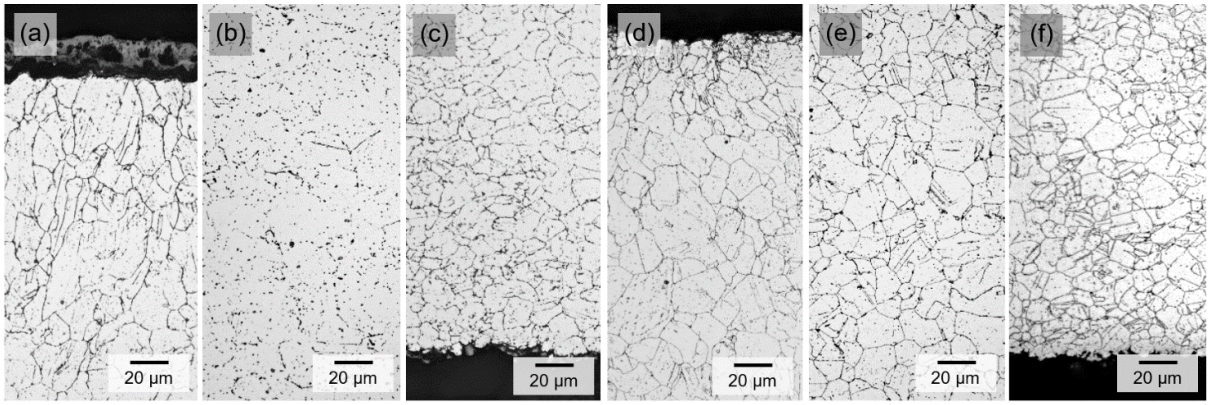

Figure 5 LOM images where the order is: outer surface, core, inner surface
of the tension side of the (a)-(c) bend A and (d)-(f) bend B

At temperatures around 550 °C, according to the phase diagrams [5], it is also possible to discover a brittle intermetallic Fe-Cr-Ni sigma phase but according to the literature [6] and [7], it is more likely to occur at temperatures above 650 °C. The reduction of this limit can be according to [8] caused by residual stress in the material, e.g. after welding or bending. Since the loop consists of two bends that were not annealed after bending, extra attention was paid to this area of the loop.

As shown in **Figure 6** and the EDS map of the chemical composition, the carbidic particles in the bend B are formed around the primary Nb-based particle, as well as other particles (marked in **Figure 6** with red arrow)

containing mainly Fe and then probably Ni or Mn. Cr and C are not present in the particle according to the EDS map, but because of the detection limits, there may only be a trace amount of them in the particle.

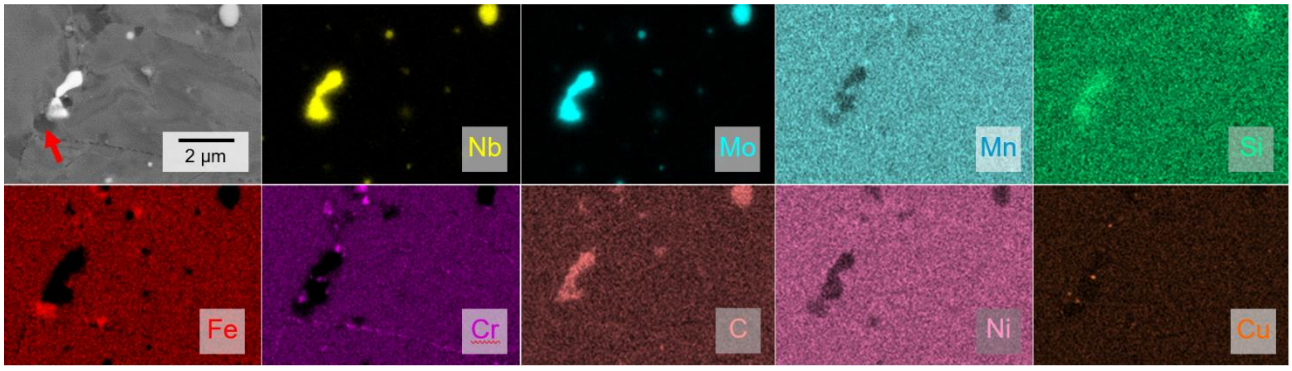

Figure 6 EDS map of the chemical composition in the core of the tensile part of the bend B

The inner surface of the loop was exposed to a water vapor environment. Macro images of the inner surface (**Figure 7**b) showed a different coloring of the corrosion layer than in the case of the outer surface (**Figure 7**a). The average thickness of the oxide layer on the inner surface was 9 µm, on the outer surface it was 14,5 µm. Near manual welds A-58 (**Figure 7**c) and A-1 (**Figure 7**d), local intergranular corrosion attack was observed along sensitized grain boundaries.

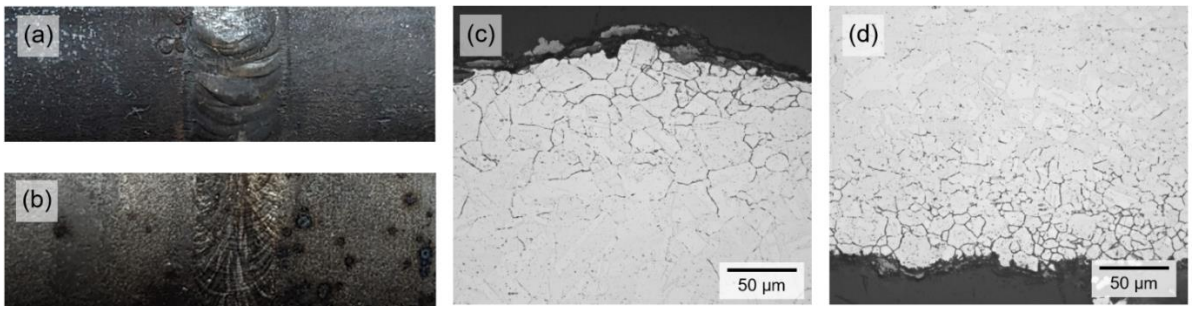

Figure 7 Welded joints and their (a) macrograph of the outer surface, (b) macrograph of the inner surface. (c) Weld A-58 corrosion near the weld, outer surface and (d) weld A-1 corrosion near the weld, inner surface.

3.4. Hardness mapping

The base material of SUPER 304H steel in as-received state has a value of (176±5) HV10. The hardness was measured along the circumference in three lines. As shown in **Figure 8** by comparing the top cross sections of the bends of the base material and the exposed bends from the exposure loop, the strengthening pattern remains the same regardless of exposure. The increase in hardness is probably caused by precipitation at the austenitic grain boundaries.

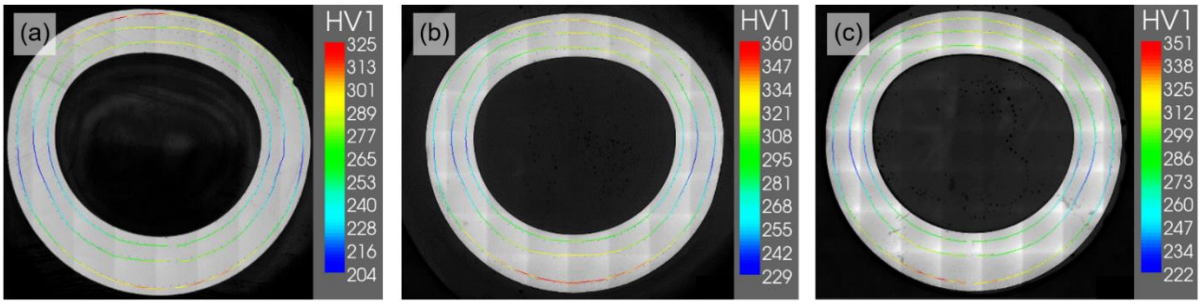

Figure 8 HV1 microhardness maps in three lines (a) bend without exposure, (b) bend A and (c) bend B

4. CONCLUSIONS

- The exposure loop enables to expose superheater parts (bends, welds) to an environment of air, water vapor and corrosive ash at the same time. During this experiment, in contrast to long-term isothermal annealing, it is subjected not only to temperature, but also to internal overpressure.
- The exposure loop made of SUPER 304H steel was operated at 550 °C for 10,000 h with internal pressure of 23.2 MPa. In the microstructure, events corresponding to the operation of a power plant were simulated.
- The exposure loop offers possibilities for other analyzes beyond the scope of this article – Charpy impact test of selected parts, analysis of the corrosion layer, depth of corrosion attack around the weld joints and comprehensive mechanical testing of the stripe-shaped specimens sealed in the body of the loop.

ACKNOWLEDGEMENTS

This article was supported from the state budget by the Czech Republic Technology Agency under the THÉTA 5 Program, project no. TK05020109.

REFERENCES

[1] TŘEŠŇÁK P. Aktualizace státní energetické koncepce. In: *Jak státní energetické koncepce ovlivní budoucnost české energetiky.* Prague: Institut pro veřejnou diskusi. 15.5.2024. Available from: https://www.youtube.com/live/T0cMbsGPNtg

[2] *Čtvrtletní zpráva o provozu elektrizační soustavy České republiky IV. Q 2024*. Jihlava, Czech republic: Energetický regulační úřad, 2024. Available from: https://eru.gov.cz/ctvrtletni-zprava-o-provozu-elektrizacni-soustavy-cr-za-iv-ctvrtleti-2023

[3] *Inspection certificate of SUPER 304H steel*. Amgasaki, Japan: Sumitomo Metals Industries, 2012. Certificate No. 030034A12.

[4] HWANG, J. H., SONG, G. D., KIM, D.-W. Tensile and fatigue properties of Super304H welded joint at elevated temperatures. *International Journal of Fatigue*. 2021, vol. 143, pp. 1-13. DOI: 10.1016/j.ijfatigue.2020.105989

[5] HORVÁTH, J. Prague, 2018. The structural stability of creep resistant austenitic steels SUPER 304H and Tp 347HFG. Dissertation. Czech Technical University in Prague.

[6] ZIELIŃSKI, A., R. WERSTA, R., SROKA, M. The study of the evolution of the microstructure and creep properties of Super 304H austenitic stainless steel after aging for up to 50,000 h. *Archives of Civil and Mechanical Engineering*. 2022, vol. 22, pp. 1-24. DOI: 10.1007/s43452-022-00408-6.

[7] HUANG, X., ZHOU, Q., WANG, W. Microstructure and property evolutions of a novel Super304H steel during high temperature creeping. *Materials at High Temperatures*. 2018, vol. 35, pp. 438-450. DOI: 10.1080/09603409.2017.1376831.

[8] ZHOU, Q., LIU, J., GAO, Y. An insight into oversaturated deformation-induced sigma precipitation in Super304H austenitic stainless steel. *Materials & Design*. 2019, vol. 181, pp. 1-11. DOI: 10.1016/j.matdes.2019.108056.